What Controls the Lamellar Orientation at the Surface of Polymer Films during Crystallization?

Yong Wang,[†] Chi-Ming Chan,*[,†] and Kai-Mo Ng[†,‡]

Department of Chemical Engineering and Advanced Engineering Materials Facility, Hong Kong University of Science and Technology, Clear Water Bay, Hong Kong

Lin Li

State Key Laboratory of Polymer Physics and Chemistry, Center for Molecular Science, Institute of Chemistry, Chinese Academy of Sciences, Beijing 100080, China

Received September 24, 2007; Revised Manuscript Received December 27, 2007

ABSTRACT: The crystalline morphologies of poly(bisphenol A hexane ether) (BA-C6) films were investigated using atomic force microscopy (AFM). The glass transition temperatures (T_gs) of the BA-C6 films on silicon wafers were determined using an ellipsometer, and the results indicated that the T_g increased dramatically when the thickness of the films was smaller than about 30 nm. The lamellar orientation of the BA-C6 films with thicknesses of about 33 and 970 nm was studied at temperatures varying between the T_g and the melting point of the polymer (T_m). In the 33 nm films, we found that the edge-on lamellae predominantly formed at the temperatures close to the bulk T_g ($T_g \sim 35$ °C), while some edge-on and mostly flat-on lamellae developed at the temperatures near T_m ($T_m \sim 98$ °C). In addition to temperature, the film thickness was found to have significant influence on the observed lamellar orientation at the surface. The concentration of the edge-on lamellae increased as the film thickness increased. These observations were explained on the basis that polymer chain mobility is strongly affected by the thickness of the films, temperature, and the interactions between the polymer and substrate. A three-layer T_g model was proposed for supported polymer films.

Introduction

It is well-known that polymer chains in ultrathin films (thickness <100 nm) have significantly different structures and properties from those in thick films and bulk polymers.[1–26] Polymer thin and ultrathin films are important to many applications such as adhesion, surface wetting and dewetting, and liquid crystal alignment.

Many studies on amorphous polymers have shown that polymer chains in the vicinity of the interface between the film and the substrate as well as near the surface are different from those in the bulk.[3–8] At or near the polymer/air interface (surface) of a polymer film, the mobility of the polymer chains is higher than that in the bulk. In contrast, the positive interactions between polymer chains and solid substrates often retard chain mobility. Computer simulations have shown an enrichment of the chain ends at the surface.[13–16] These chains exhibit a strong tendency to orient with their longest dimension parallel to the film's surface. The mass density near the surface gradually drops to zero, displaying the characteristic sigmoidal shape. At the polymer and substrate interface, computer simulations indicated that the presence of confining walls results in an increase in the mass density, and the longest dimensions of the chains are oriented parallel to the substrate.[14,16] Many experimental measurements of the glass transition temperature (T_g) of supported polymer films indicated that there exist a lower T_g layer near the film surface and a higher T_g layer near the substrate.[9–12,17–26] The combined effects of the lower T_g layer at the surface and the higher T_g layer at the polymer and substrate interface increase or decrease the apparent T_g of thin and ultrathin films.

The crystallization behaviors of crystalline polymers in thin and ultrathin films have also attracted much interest. For instance, Schonherr et al.[27] imaged thin and thick crystallized films of poly(ethylene oxides) (PEO) and showed that when the film thickness was greater than 1000 nm, the lamellae were oriented edge-on (their *c*-axis was parallel to the film substrate), while in the films thinner than 300 nm, the crystals were mainly composed of flat-on lamellae (their *c*-axis was normal to the film substrate). Using in-situ grazing incidence X-ray diffraction, Jukes et al.[28] reported a fast crystal growth rate of poly(ethylene terephthalate) (PET) in the region near the surface of thin films. Reiter et al.[29–31] studied the morphology of PEO in the quasi-two-dimensional crystals (branched crystalline structure) formed at the edge of dewetting droplets. A lattice model was proposed by Reiter and Sommer[30] for the polymer crystal growth in two dimensions where the chains were considered to be the smallest units in the crystallization process and the crystal growth was diffusion-limited (i.e., the crystals were diffusion-controlled aggregates[32]). Also, Lovinger et al.[33] observed single crystals grown from the melt of poly(trifluoroethylene) and discussed the morphology on the basis of the diffusion-controlled aggregates.[32] Monte Carlo simulations indicated that, at high temperatures, edge-on lamellae develop predominantly in thin films with repulsive substrates while flat-on lamellae exist mainly in thin films with strong interactions with their substrates.[34]

Although these studies extended our insights into the polymer crystallization behaviors of thin and ultrathin films, a comprehensive understanding of lamellar orientation in ultrathin and thin films is still lacking because most past studies did not focus on the strong influence of the film surface and the interface between the substrate and the film as well as the simultaneous effects of crystallization temperatures and film thickness on the crystallization behaviors. As a result, some common but very important issues in polymer film crystallization have not been clearly described. For example, what roles do the film surface and the interface between the substrate and the film play in the crystallization and development of surface morphology at

* Corresponding author. E-mail: kecmchan@ust.hk.
† Department of Chemical Engineering.
‡ Advanced Engineering Materials Facility.

10.1021/ma7021309 CCC: $40.75
Published on Web 03/04/2008

temperatures between T_g and T_m? In comparison with thick polymer films (normally with film thicknesses >1 μm), ultrathin films offer a great opportunity to study the influence of the film surface and interface on the crystallization behavior because of the increasing influence of the two interfaces of the ultrathin films as the film thickness decreases.

It is well-known that polymer crystallization initiates either homogeneously or heterogeneously. Lamellae with the edge-on and flat-on orientations are commonly observed on the surfaces of films. When homogeneous nucleation occurs at a film's surface, the edge-on orientation is preferred because the surface free energy of the crystal's lateral surface has a much smaller surface free energy than that of the crystal's fold surface.[35] On the other hand, when heterogeneous nucleation occurs at the polymer/substrate interface of polymer films, the flat-on orientation is favored.[36]

In recent years, the study of the crystallization behaviors of polymers using atomic force microscopy (AFM) has become popular due to the ability of AFM to obtain in-situ and real-time structural information at the nanometer level.[37–50] As we previously reported,[43–49] real-time AFM observations of the formation of spherulites, which mainly consist of edge-on lamellae, suggested that a spherulite (or a crystal aggregate) starts with the birth of an embryo, which develops into a founding lamella. Through branching and splaying, the founding lamella then grows into a lamellar sheaf and then finally forms a mature spherulite.

In this study, tapping mode AFM (TM-AFM) was employed to study the crystallization behavior of poly(bisphenol A hexane ether) (BA-C6) and poly(bisphenol A octane ether) (BA-C8) thin films in a temperature range from their T_gs to their T_ms. The T_g of the films on silicon wafer substrates was measured as a function of film thickness by an ellipsometer. It was found that the T_g of the BA-C6 films increased dramatically when the film thickness was smaller than 30 nm. The morphologies of the films with thicknesses similar to this critical value were studied as a function of the temperature ranging between T_g and T_m. The factors that control the surface morphology of the films were thereby determined.

Experimental Section

Poly(bisphenol A hexane ether) (BA-C6) was synthesized by condensation polymerization of bisphenol A and 1,6-dibromohexane. We used 1,6-dibromohexane as the excess component to produce a polymer with Br in the end groups. The molecular characteristics of the BA-C6 samples were determined using gel permeation chromatography at room temperature with tetrahydrofuran as the solvent. The thermal analysis of the sample was conducted using a Perkin-Elmer Pyris Diamond differential scanning calorimeter (DSC), which was calibrated using indium. DSC measurements were performed under nitrogen at a heating rate of 10 °C/min. The number-average molecular weight ($\bar{M}_n$), the weight-average molecular weight ($\bar{M}_w$), the polydispersity index ($\bar{M}_w/\bar{M}_n$), the glass transition temperature (T_g), and the melting point (T_m) of the BA-C6 sample were determined to be 12 400 g/mol, 21 800 g/mol, 1.76, 35.1 °C, and 98.1 °C, respectively.

The substrates were silicon wafers. They were cleaned in a mixture of H_2SO_4 and H_2O_2 (70/30 vol %) for 30 min at 100 °C. After cooling to room temperature, the substrates were thoroughly washed with deionized water and then dried under a stream of nitrogen. The water contact angle on the cleaned substrates was less than 5°.

Ultrathin BA-C6 films with different thicknesses were prepared using 1 to 10 mg mL^{-1} polymer−chloroform solutions at 3000−5000 rpm spin-coating speeds for 30 s. The film samples were dried in a vacuum oven at room temperature for 15 min before any of the experiments and thickness measurements. The thickness of amorphous BA-C6 films was estimated by a single-wavelength (He Ne laser), null-type ellipsometer (Gaertner Co.; Model L116C). The thicknesses at three locations in each film were measured, and only films with thickness errors less than 10% were used. In addition to the single-wavelength null-type ellipsometer, a variable-angle rotating analyzer spectroscopic ellipsometer (J.A. Woollam Co.; H-VASE) was also used to measure the T_g of the ultrathin amorphous BA-C6 films. The T_g of the film was measured as a function of thickness. For each film thickness five film samples were used. A heating stage was developed to be used in conjunction with the H-VASE. To be certain that the BA-C6 film samples had a similar and well-defined thermal history, all samples were annealed for 24 h at 35 °C (close to the sample's bulk T_g) in an oven before the T_g measurement. Because of the low crystallization rate of this polymer, no crystal was observed by AFM in the ultrathin films after 24 h of annealing. The ellipsometric angles were continuously monitored while the film sample was being heated at a constant rate of 1 °C/min from 21 to 100 °C. Films were annealed in an oven at various temperatures as well as for different periods of time.

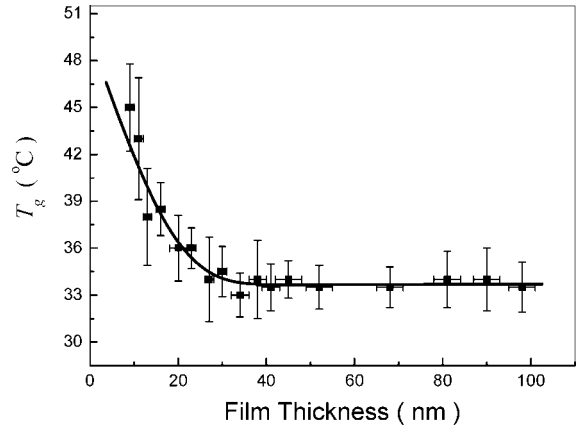

Figure 1. Measured T_gs of ultrathin BA-C6 films as a function of film thickness.

TM-AFM images were obtained using a NanoScope III Multi-Mode AFM (Digital Instruments) equipped with a high-temperature heater accessory (Digital Instruments). Both height and phase images were recorded simultaneously using the retrace signal. Si tips (TESP) with a resonance frequency of ~300 kHz and a spring constant of about 40 N m^{-1} were used and the scan rate ranged from 0.4 to 1.2 Hz/s with the scanning density of 512 lines/frame. The set-point amplitude ratio, r_{sp} ($r_{sp} = A_{sp}/A_0$, where A_{sp} is the set-point amplitude and A_0 is the amplitude of the free oscillation, which was always 2.0 V (about 68 nm) in this study), was adjusted to be as large as possible for normal observations, which was often in the range from 0.7 to 0.9.

Results

Ellipsometry is widely used for measuring T_g of polymer thin films by detecting the volumetric change during the transition of the polymer from the glassy to the rubbery state as the temperature increases. In ellipsometric measurements, the ellipsometric angle is linear with temperature in either the glassy or rubbery state; thus, the point at which the two straight lines intersect gives T_g of the polymer film.[10,12,19–22] Figure 1 shows the plot of the measured T_gs of ultrathin BA-C6 films as a function of film thickness, clearly indicating that the T_g is strongly dependent on the thickness. The value of T_g remains at about 33.8 °C and sharply increases after the thickness is smaller than about 30 nm. This result is in good agreement with the results of many previous studies on supported polymer films with strong interactions with their substrates.[9–12]

Figure 2 displays a set of AFM images of the crystalline morphologies of the ultrathin BA-C6 films at crystallization temperatures (T_c), namely 45, 60, 75, and 90 °C, which

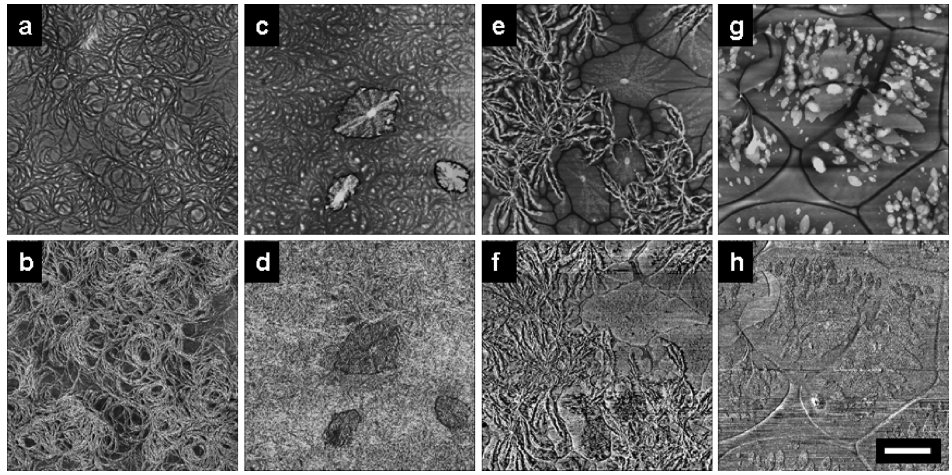

Figure 2. A set of AFM images. Height and phase images are in the upper and lower rows, respectively. The images show the crystalline morphologies in ultrathin BA-C6 films crystallized at 45 (a), 60 (c), 75 (e), and 90 °C (g). The film thickness and crystallization time were about 33 ± 3 nm and 84 h, respectively. The scale bar in (h) represents 10 μm.

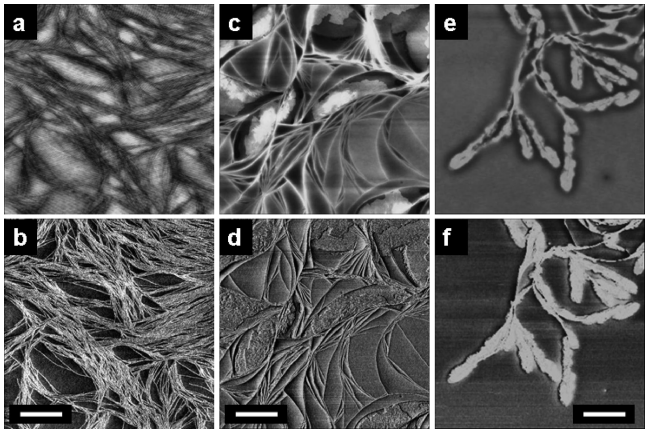

Figure 3. A series of higher resolution AFM images of the ultrathin BA-C6 films crystallized at 45 (a), 60 (c), and 75 °C (e) shown in Figure 2. Height and phase images are in the upper and lower rows, respectively. The scale bars in (b), (d), and (f) represent 1, 1, and 2 μm, respectively.

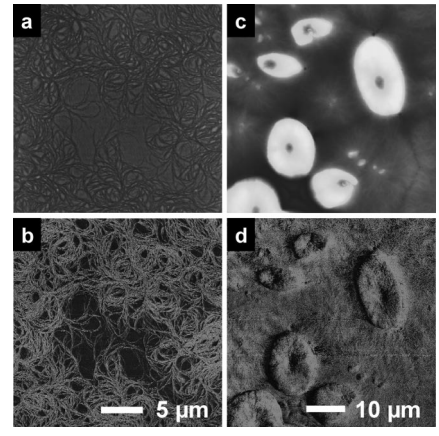

Figure 4. Two pairs of AFM images, height images (upper row) and phase images (lower row), showing the crystalline morphologies of the thick BA-C6 films crystallized at 45 (a) and 90 °C (c). The film thickness and annealing time were about 970 ± 60 nm and 72 h, respectively.

correspond respectively to the images shown in Figures 2a,b, c,d,e,f, and g,h. The film thicknesses of the samples shown in Figure 2 were about 33 ± 3 nm and were purposely chosen to be close to the threshold thickness at which T_g increases dramatically. The annealing time was ~84 h. Figures 2a,c,e, and g are height images, and Figures 2b,d,f, and h are phase images. Figures 2a,b show that, at 45 °C, only edge-on lamellae are present and no flat-on crystals can be seen. At 60 °C, in addition to many edge-on lamellae, a few sporadic flat-on crystals are observed, as shown in Figures 2c,d. More and more flat-on crystals are formed at higher temperatures, such as 75 and 90 °C. As shown in Figures 2g,h, at 90 °C the flat-on crystals occupy almost the full images and only a few edge-on lamellae can be seen. These results clearly indicate that edge-on lamellae are likely to form at lower temperatures, while flat-on lamellae are the preferred orientation at higher temperatures.

At 45, 60, and 75 °C, remarkable morphological differences were found in the higher resolution AFM height and phase images of the 33 nm thick BA-C6 films after 84 h of annealing, as shown in Figure 3. The height and phase images are in the upper and lower rows, respectively. While only edge-on lamellae are seen in Figures 3a,b, some relatively small flat-on crystals, which appear beside the previously developed edge-on lamellae, can be clearly seen in Figures 3c,d. In Figures 3e,f, many small flat-on crystals, which form beside the previously produced edge-on lamellae, are observed and some of them have enclosed the growing tips of the edge-on lamellae, resulting in growth cessation of the edge-on lamellae.

Different crystalline morphologies from those observed in the ultrathin films are expected in thick BA-C6 films because the impact of the polymer/substrate interface on the crystalline morphologies at the film's surface diminishes as the thickness increases. Figure 4 presents two sets of AFM images—height images (upper row) and phase images (lower row)—showing the crystalline morphologies of thick BA-C6 films crystallized at 45 and 90 °C. The thickness of the films was measured to be about 970 ± 60 nm, and the annealing time was ~72 h. At 45 °C (cf. Figures 4a,b), only the edge-on lamellae are seen. However, at 90 °C (cf. Figures 4c,d), many spherulites with edge-on lamellae were detected along several circular objects consisting of flat-on lamellae. We observed an increase in the concentration of the edge-on lamellae as the thickness of the film increased even at high temperatures.

These phenomena were observed not only in ultrathin BA-C6 films but also in the ultrathin films of other poly(bisphenol A alkyl ether) (BA-C*n*), such as poly(bisphenol A octane ether) (BA-C8), poly(bisphenol A decane ether) (BA-C10), and poly(bisphenol A dodecane ether) (BA-C12). Figure 5 shows a set of AFM images of a BA-C8 sample ($\bar{M}_n$, $\bar{M}_w/\bar{M}_n$, T_g, and

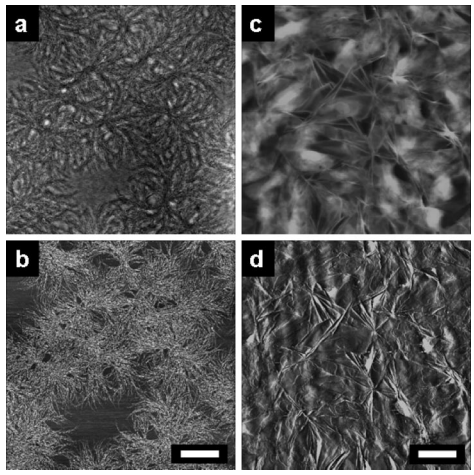

Figure 5. Two pairs of AFM images, height images (upper row) and phase images (lower row), showing the crystalline morphologies of the ultrathin BA-C8 films crystallized 30 (a) and 80 °C (c). The film thickness and annealing time were about 39 ± 2 nm and 96 h, respectively. The scale bars in (b) and (d) represent 5 and 3.3 μm, respectively.

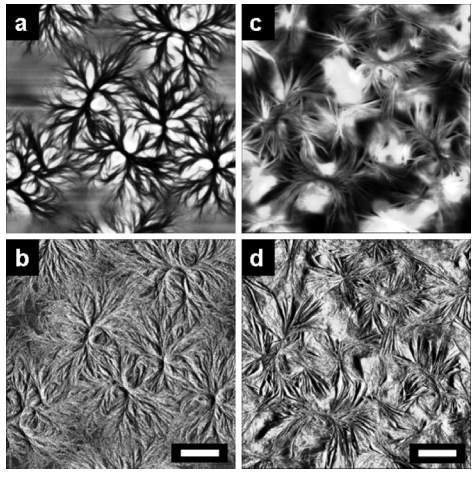

Figure 6. Two pairs of AFM images, height images (upper row) and phase images (lower row), showing the crystalline morphologies of the thick BA-C8 films crystallized at 30 (a) and 80 °C (c). The film thickness and annealing time were about 1050 ± 50 nm and 72 h, respectively. The scale bars in (b) and (d) represent 5 and 3.3 μm, respectively.

T_m of this sample are 19 800 g/mol, 1.42, 19.6 °C, and 84.4 °C, respectively) crystallized at 30 and 80 °C, which are close to its T_g and T_m, respectively. The thickness of the films was determined to be about 39 ± 2 nm, and the annealing time was ~96 h. The height and phase images are in the upper and lower rows, respectively. At 30 °C, only the edge-on lamellae are detected (cf. Figures 5a,b), while crystallized at 80 °C, both edge-on and flat-on lamellae are found (cf. Figures 5c,d). Figure 6 presents two sets of AFM images—height images (upper row) and phase images (lower row)—showing the crystalline morphologies of thick BA-C8 films crystallized at 30 and 80 °C. The thickness of the films was measured to be about 1050 ± 50 nm, and the annealing time was ~72 h. At 30 °C (cf. Figures 6a,b), only edge-on lamellae are seen, while at 80 °C (cf. Figures 6c,d), some edge-on and flat-on lamellae are detected. An increase in the concentration of the edge-on lamellae is detected as the thickness of the films increases at 80 °C (cf. Figures 5c,d and 6c,d).

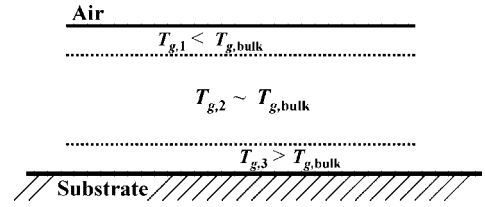

Figure 7. Schematic drawing of a three-layer T_g model of a polymer film.

Discussion

The chain mobility and T_g of a thin film vary as a function of depth into the sample due to the presence of the polymer/air and polymer/substrate interfaces.[1–26] Generally speaking, a thin film on a substrate can be considered to consist of three layers with different molecular mobilities or with different T_gs.[9] A higher chain mobility polymer layer is present at the surface due to the chain-end segregation to the film surface and the drop of the mass density from its bulk value to practically zero. If there are strong interactions between the chains and the substrate, then the chain mobility at the polymer/substrate interface is lower than that in the bulk. The interactions between the polymer chains and the substrate severely retard the motion of the chains, resulting in the formation of a higher T_g layer near the substrate. These two effects cause the formation of three layers of polymer with different T_gs in the film: a layer near the film surface with a lower T_g, another layer near the interface between the polymer film and the substrate with a higher T_g and the third layer sandwiched between these two layers with the bulk T_g. The dependence on thickness of the T_g of the BA-C6 films, as shown in Figure 1, indicates that the interactions between BA-C6 chains and silicon wafer substrates are strong because a sharp increase in the value of T_g of the film is observed when the thickness is smaller than about 30 nm. A schematic diagram showing the three-layer T_g model of a polymer film is presented in Figure 7.

It is generally accepted that the plot of the primary nucleation rate as a function of temperature is a bell-shaped curve with a maximum value at a temperature between T_g and T_m,[51] as shown in Figure 8a. In the three-layer T_g model, there exist three layers with $T_g = T_{g,1}$, $T_{g,2}$ (or $T_{g,bulk}$), and $T_{g,3}$ in BA-C6 films. Because $T_{g,3}$ is much higher than $T_{g,1}$, the primary nucleating rates as a function of temperature of these three layers are different. The temperature at which the maximum nucleation rate occurs in the $T_{g,1}$ layer is lower than that in the $T_{g,3}$ layer. In this case, the nucleation rates of these two layers at a certain T_c differ significantly, as shown in Figure 8d.

According to a simple thermodynamic model, edge-on or flat-on lamellae are predicted to form in thick and ultrathin films, respectively.[35,36] However, we cannot generalize this observation without considering the kinetic effects of nucleation, which plays a dominant role in determining the orientation of the lamellae formed in thin films. On the basis of the three-layer T_g model, the primary nucleation rate of the layer near the film surface has a maximum value at low temperatures when compared with the primary nucleation rate of the layer near the film/substrate interface. At low temperatures, edge-on lamellae with the highest nucleation rate are predicted to be present predominantly at the surface because the polymer chains at the surface, which exhibit a strong tendency to orient with their longest dimension parallel to the film's surface,[13–16] have the highest mobility. Experimentally, we and other researchers have observed spherulites with two eyes and spherical symmetry formed at the surface of polymer films.[37,46,47] If nuclei are formed in the bulk, spherulites with two eyes and spherical symmetry would not appear at the surface. In addition, the appearance and disappearance of

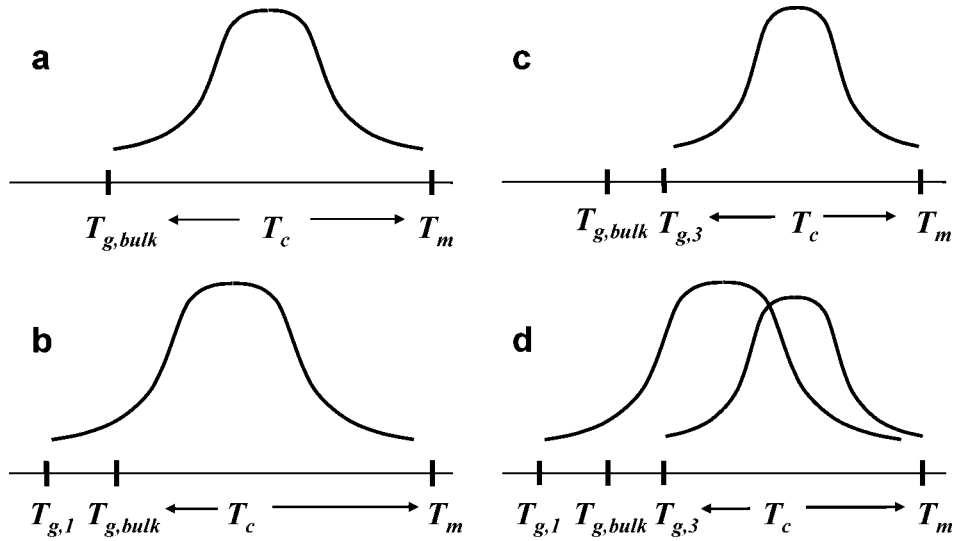

Figure 8. (a) A bell-shaped curve shows the primary nucleation rate as a function of temperature. (b) A bell-shaped curve shows the primary nucleation rate of the polymer in the layer with $T_g = T_{g,1}$ near the surface in the temperature window from $T_{g,1}$ to T_m. (c) A bell-shaped curve shows the primary nucleation rate of the polymer in the layer with $T_g = T_{g,3}$ near the polymer/substrate interface in the temperature window from $T_{g,3}$ to T_m. (d) shows the combination of (b) and (c).

embryos at the surface of polymer films further confirm that nucleation preferably occurs at the surface.[45,46] The proposed three-layer T_g model was confirmed by observations that mostly edge-on lamellae were found on a 33 nm thick film at lower temperatures, such as 45 and 60 °C, as shown in Figures 2a,b and c,d, while higher concentrations of flat-on lamellae were detected at higher temperatures, such as 75 and 90 °C, as shown in Figures 2e,f and g,h. When crystallized at low T_c s close to bulk T_g, the homogeneous nucleation rate of the edge-on lamellae at the film surface is faster than the heterogeneous nucleation rate of the flat-on lamellae at the polymer/substrate interface.

At 75 °C, a mixture of edge-on and flat-on lamellae is observed (see Figures 2e,f), and the enclosure of some of the edge-on lamellae by the later-produced flat-on lamellae is also observed in the higher resolution images (see Figures 3e,f). At 75 °C, we can deduce that both homogeneous and heterogeneous nucleation can occur in appreciable rates because of the presence of both edge-on and flat-on lamellae. After the formation of edge-on lamellae at the surface, the lamellae can propagate parallel as well as perpendicularly to the surface. Because the thickness of this film was only 33 nm, the edge-on lamellae would not need long times to reach the polymer/substrate interface or the fold surface of flat-on lamellae growing upward from the interface. Crystal defects such as chain loops and cilia and screw dislocations are the direct causes of lamellar branching.[44–49,52,53] Further branching of the edge-on lamellae due to the presence of loose loops and protruding cilia at the polymer/substrate interface or at the fold surface of the flat-on lamellae will easily lead to the formation of induced flat-on nuclei, as shown schematically in Figure 9. The growth of these flat-on lamellae in the directions parallel and perpendicular to the surface will eventually lead to the enclosure of the edge-on lamellae due to the fact the growth rate of the flat-on lamellae is much faster than that of the edge-on lamellae in thin films as observed in this work and predicted by Ma et al.[34]

As the film thickness increases, the concentration of the flat-on lamellae decreases even at 90 °C for BA-C6, as shown in Figure 4, and at 80 °C for BA-C8, shown in Figure 6. At high temperatures, the heterogeneous nucleation rate at the polymer/substrate interface is faster than the homogeneous nucleating rate at the film surface; however, it will take much longer times for the flat-on lamellae, which have originated at the polymer/substrate interface, to grow and show up at the surface when the film is thick. Hence, we expect to observe a higher concentration of edge-on lamellae when the thickness of the film increases at all temperatures.

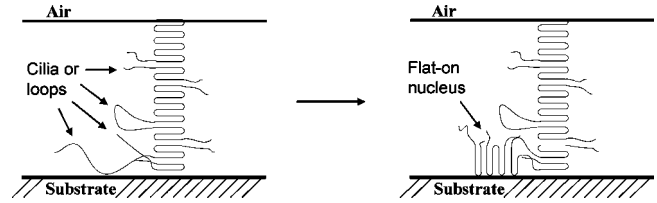

Figure 9. Schematic illustration of the formation of an induced flat-on nucleus at the polymer/substrate interface next to an edge-on lamella.

Our model can be used to explain many results reported in the literature.[27,36,54–60] For example, in the crystallization studies of PEO,[27] linear low-density polyethylene (PE)[36] and poly(di-*n*-hexylsilane),[54] the transition of crystal orientation from the edge-on orientation to the flat-on orientation was observed as the film thickness decreased. In addition, many research groups showed that edge-on crystals were found predominantly in relatively thick PET[55] and PE[57,58] films, while flat-on crystals were observed predominantly in PET[56] and PE[59,60] ultrathin films. In a dynamic Monte Carlo simulation, Ma et al.[34] predicted that edge-on lamellae exist predominantly at the interface between a polymer and a slippery wall (repulsive wall) due to crystal nucleation near the wall, while flat-on lamellae are dominant when there are strong interactions between the polymer and substrate due to strong inhabitation of the thickening growth of the edge-on lamellae. If we treat that the polymer near the film surface is similar to the polymer near a slippery wall, then there is some agreement between our results and that of Ma et al.[34] Our model also predicts the dominance of the flat-on lamellae in ultrathin films when there are strong interactions between the polymer and the substrate. This also agrees with the results predicted by the simulation of Ma et al.,[34] except we believe that nucleation is the controlling mechanism. In addition, our model can explain the coexistence of both edge-on and flat-on lamellae at the surface as well as the case where edge-on lamellae are formed on the fold surface of flat-on lamellae. The increase in the concentration of edge-on lamellae as the film thickness increases and the increase in

the concentration of flat-on lamellae as temperature increases can also be predicted with our model.

Conclusion

The T_g of BA-C6 films was found to remain constant as a function of thickness and to increase dramatically when the film thickness was smaller than about 30 nm. The formation of edge-on lamellae was preferred at lower temperatures close to the T_g of the polymer, while both edge-on and flat-on lamellae were detected at higher temperatures near the T_m of the polymer. A simple thermodynamic model cannot correctly predict the lamellar orientation of polymer films. Polymer chain mobility, temperature, film thickness, and the interactions between the polymer and substrate are important parameters to be considered for correct predictions. A three-layer T_g model was proposed to explain the predominance of edge-on lamellae observed at the surface of ultrathin films at low temperatures and the increase in the concentration of the flat-on lamellae as the temperature increases. At low temperatures, edge-on lamellae develop at the surface because the homogeneous nucleation is the quickest at the surface of the film. At high temperatures, the heterogeneous nucleation rate at the polymer/substrate is higher than the homogeneous nucleation rate at the surface. Consequently, more flat-on lamellae are observed at the surface. At very high temperatures, the primary homogeneous nucleation rate at the surface becomes very small and the surface is then mostly filled with flat-on lamellae that have originated at the interface between the polymer and the substrate. However, at large film thicknesses, the concentration of the edge-on lamellae will increase even at very high crystallization temperatures because it takes a long time for the flat-on lamellae, which have originated at the interface between the polymer and substrate, to appear at the surface. Therefore, large thicknesses will favor the observation of the edge-on lamellae at the surface.

Acknowledgment. We are grateful for support from the Hong Kong Government Research Grants Council under Grants 600405 and 600503.

References and Notes

(1) Frank, C. W.; Bao, V.; Despotopoulou, M. M.; Pease, R. F. W.; Hinsberg, W. D.; Miller, R. D.; Rabolt, J. F. *Science* **1996**, *273*, 912.
(2) Sanchez, I. C., Ed.; *Physics of Polymer Surfaces and Interfaces*; Butterworth-Heinemann: Boston, MA, 1992.
(3) Calvert, P. *Nature (London)* **1996**, *384*, 311.
(4) Jones, R. L.; Kumar, S. K.; Ho, D. L.; Briber, R. M.; Russell, T. P. *Nature (London)* **1999**, *400*, 146.
(5) Zheng, X.; Rafailovich, M. H.; Sokolov, J.; Strzhemechny, Y.; Schwarz, S. A.; Sauer, B. B.; Rubinstein, M. *Phys. Rev. Lett.* **1997**, *79*, 241.
(6) Zheng, X.; Sauer, B. B.; van Alsten, J. G.; Schwarz, S. A.; Rafailovich, M. H.; Sokolov, J.; Rubinstein, M. *Phys. Rev. Lett.* **1995**, *74*, 407.
(7) Frank, B.; Gast, A. P.; Russell, T. P.; Brown, H. R.; Hawker, C. *Macromolecules* **1996**, *29*, 6531.
(8) Lin, E. K.; Kolb, R.; Satija, S. K.; Wu, W.-L. *Macromolecules* **1999**, *32*, 3753.
(9) DeMaggio, G. B.; Frieze, W. E.; Gidley, D. W.; Zhu, M.; Hristov, H. A.; Yee, A. F. *Phys. Rev. Lett.* **1997**, *78*, 1524.
(10) Keddie, J. L.; Jones, R. A. L.; Cory, R. A. *Faraday Discuss.* **1994**, *98*, 219.
(11) Van Zanten, J. H.; Wallace, W. E.; Wu, W. *Phys. Rev. E* **1996**, *53*, R2053.
(12) Grohens, Y.; Brogly, M.; Labbe, C.; David, M. O.; Schultz, J. *Langmuir* **1998**, *14*, 2929.
(13) Theodorou, D. N. *Macromolecules* **1989**, *22*, 4578.
(14) Mansfield, K. F.; Theodorou, D. N. *Macromolecules* **1991**, *24*, 4295.
(15) Mansfield, K. F.; Theodorou, D. N. *Macromolecules* **1990**, *23*, 4430.
(16) Harmandaris, V. A.; Kaoulas, K. C.; Mavrantzas, V. G. *Macromolecules* **2005**, *38*, 5796.
(17) Reiter, G. *Europhys. Lett.* **1993**, *23*, 579.
(18) Seki, T.; Fukuda, K.; Ichimura, K. *Langmuir* **1999**, *15*, 5098.
(19) Kawana, S.; Jones, R. A. L. *Phys. Rev. E* **2001**, *63*, 021501.
(20) Kim, J. H.; Jang, J.; Zin, W.-C. *Langmuir* **2000**, *16*, 4064.
(21) Kim, J. H.; Jang, J.; Zin, W.-C. *Langmuir* **2001**, *17*, 2703.
(22) Keddie, J. L.; Jones, R. A. L.; Cory, R. A. *Europhys. Lett.* **1994**, *27*, 59.
(23) Forrest, J. A.; Dalnoki-Veress, K.; Stevens, J. R.; Dutcher, J. R. *Phys. Rev. Lett.* **1996**, *77*, 2002.
(24) Forrest, J. A.; Dalnoki-Veress, K.; Dutcher, J. R. *Phys. Rev. E* **1997**, *56*, 5705.
(25) Meyers, G. F.; DeKoven, B. M.; Seitz, J. T. *Langmuir* **1992**, *8*, 2330.
(26) Jean, Y. C.; Cao, Z. H.; Yuan, J.-P.; Huang, C.-M.; Nielsen, B.; Asoka-Kuma, P. *Phys. Rev. B* **1997**, *56*, R8459.
(27) Schonherr, H.; Frank, C. W. *Macromolecules* **2003**, *36*, 1188.
(28) Jukes, P. C.; Das, A.; Durell, M.; Trolley, D.; Higgins, A. M.; Geoghegan, M.; Macdonald, J. E.; Jones, R. A. L.; Brown, S.; Thompson, P. *Macromolecules* **2005**, *38*, 2315.
(29) Reiter, G.; Sommer, J. U. *J. Chem. Phys.* **2000**, *112*, 4376.
(30) Reiter, G.; Sommer, J. U. *J. Chem. Phys.* **2000**, *112*, 4384.
(31) Reiter, G.; Sommer, J. U. *Phys. Rev. Lett.* **1998**, *80*, 3771.
(32) Witten, T. A.; Sander, L. M. *Phys. Rev. Lett.* **1981**, *47*, 1400.
(33) Lovinger, A. J.; Cais, R. E. *Macromolecules* **1984**, *17*, 1939.
(34) Ma, Y.; Hu, W.; Reiter, G. *Macromolecules* **2006**, *39*, 5159.
(35) Chan, C. M.; Li, L. *Adv. Polym. Sci.* **2005**, *188*, 1.
(36) Wang, Y.; Ge, S.; Rafailovich, M.; Sokolov, J.; Zou, Y.; Ade, H.; Luening, J.; Lustiger, A.; Maron, G. *Macromolecules* **2004**, *37*, 3319.
(37) Pearce, R.; Vansco, G. J. *Macromolecules* **1997**, *30*, 5843.
(38) Hobbs, J. K.; McMaster, J. T.; Miles, M. J.; Barham, P. J. *Polymer* **1998**, *39*, 2437.
(39) Beekmans, L. G. M.; Vallée, R.; Vancso, G. J. *Macromolecules* **2002**, *35*, 9383.
(40) Zhou, W.; Cheng, S. Z. D.; Putthanarat, S.; Eby, R. K.; Reneker, D.; Lotz, B.; Magonov, S.; Hsieh, E. T.; Geerts, R. G.; Palackal, S. J.; Hawley, G. R.; Welch, M. B. *Macromolecules* **2000**, *33*, 6861.
(41) Kikkawa, Y.; Abe, H.; Iwata, T.; Inoue, Y.; Doi, Y. *Biomacromolecules* **2001**, *2*, 940.
(42) Mareau, V. H.; Prud'homme, R. E. *Macromolecules* **2005**, *38*, 398.
(43) Wang, Y.; Chan, C. M.; Ng, K. M.; Jiang, Y.; Li, L. *Langmuir* **2006**, *22*, 7384.
(44) Jiang, Y.; Yan, D. D.; Gao, X.; Han, C. C.; Jin, X. G.; Li, L.; Wang, Y.; Chan, C. M. *Macromolecules* **2003**, *36*, 3652.
(45) Lei, Y. G.; Chan, C. M.; Wang, Y.; Ng, K. M.; Jiang, Y.; Li, L. *Polymer* **2003**, *44*, 4673.
(46) Lei, Y. G.; Chan, C. M.; Li, J. X.; Ng, K. M.; Wang, Y. *Macromolecules* **2002**, *35*, 6751.
(47) Li, L.; Chan, C. M.; Li, J. X.; Ng, K. M.; Yeung, K. L.; Weng, L. T. *Macromolecules* **1999**, *32*, 8240.
(48) Li, L.; Chan, C. M.; Yeung, K.; L; Li, J. X.; Ng, K. M.; Lei, Y. G. *Macromolecules* **2001**, *34*, 316.
(49) Wang, Y.; Chan, C. M.; Ng, K. M.; Jiang, Y.; Li, L. *Langmuir* **2004**, *20*, 8220.
(50) Duan, Y. X.; Jiang, Y.; Jiang, S. D.; Li, L.; Yan, S. K.; Schultz, J. M. *Macromolecules* **2004**, *37*, 9283.
(51) Painter, P. C.; Coleman, M. M. *Fundamentals of Polymer Science*, 2nd ed.; Technomic Publishing Co.: Lancaster, PA, 1997.
(52) Bassett, D. C. *Philos. Trans. R. Soc. London* **1994**, *A348*, 29.
(53) Keith, H. D.; Padden, F. J. *J. Appl. Phys.* **1963**, *34*, 2409.
(54) Hu, Z. J.; Huang, H. Y.; Zhang, F. J.; Du, B. Y.; He, T. B. *Langmuir* **2004**, *20*, 3271.
(55) Durell, M.; Macdonald, J. E.; Trolley, D.; Wehrum, A.; Jukes, P. C.; Jones, R. A. L.; Walker, C. J.; Brown, S. *Europhys. Lett.* **2002**, *58*, 844.
(56) Sakai, Y.; Imai, M.; Kaji, K.; Tsuji, M. *Macromolecules* **1996**, *29*, 8830.
(57) Hobbs, J. K.; Humphris, A. D. L.; Miles, M. J. *Macromolecules* **2001**, *34*, 5508.
(58) Bartczak, Z.; Argon, A. S.; Cogen, R. E.; Kowalewski, T. *Polymer* **1999**, *40*, 2367.
(59) Wittmann, J. C.; Lotz, B. *J. Polym. Sci., Polym. Phys. Ed.* **1985**, *23*, 205.
(60) Keith, H. D.; Padden, F. J.; Lotz, B.; Wittmann, J. C. *Macromolecules* **1989**, *22*, 2230.

MA7021309